Advances in Experimental Cell Biology and Cell-Material Interactions

Claire M. Cobley†, Seraphine V. Wegner†, Martin Streichfuss† and Joachim P. Spatz†

† Department of Biophysical Chemistry, University of Heidelberg, Heidelberg, Germany

and

Department of New Materials and Biosystems, Max-Planck-Institute for Intelligent Systems, Stuttgart, Germany

Abstract Recent advances in the physical sciences and engineering have made it possible to measure and manipulate the mechanical and binding properties of cells in new ways. In this chapter, we will introduce this field by discussing two different experimental approaches at the interface of biology and engineering: 1) ways to measure the different types of forces generated by the actin cytoskeleton and 2) how we can probe the interactions between cells and their environment using nanostructured surfaces.

1 Introduction

A single cell could be considered the fundamental building block of life. Yet within this single unit there exist innumerable mechanisms for the cell to sense and interact with its environment. These processes involve many different types of signaling mechanisms, from molecular cues to physical forces (Alberts et al., 2008).

The primary system responsible for regulating cellular mechanics is the cytoskeleton. Far from just acting as a static scaffold to maintain the structural integrity of the cell, the cytoskeleton is a remarkably adaptive and highly dynamic structure that provides the forces necessary for the cell to move, reproduce, and react to external stimuli (Janmey, 1998). For example, it is the main determinant of the cell's stiffness and orientation and plays a key role in cellular processes such as migration and division. The cytoskeleton is composed of three structure-giving proteins, namely actin, keratin and tubulin. All three exist in monomeric and polymerized forms and can be organized into higher order structures such as bundles and networks by specific binding and crosslinking proteins. In this way simple components can become a complex, flexible system (Alberts et al., 2008).

M. Buehler, R. Ballarini (Eds.), *Materiomics: Multiscale Mechanics of Biological Materials and Structures*, CISM International Centre for Mechanical Sciences,
DOI 10.1007/978-3-7091-1574-9_5,

Over the years, experimentalists have developed a variety of tools to probe the mechanical properties of cells on different scales. For example, experimental setups have been developed to investigate a cell's response to membrane stretching (by pulling on the substrate) or to probe the cell's stiffness in different regions (through indentation with an atomic force microscopy tip) (Jungbauer et al., 2008; Huang et al., 2004). On a much smaller scale, it is also possible to isolate the individual components of the cytoskeleton, and study their fundamental mechanical properties in controlled environments outside of the cell (Streichfuss et al., 2011).

Herein, we will illustrate through case studies some of the techniques used to understand both cellular forces and cell-material interactions. We will start with one of the fundamental building blocks of the cytoskeleton, actin filaments, and build up to more complex, whole-cell interactions. We hope that in this way we can provide a flavor of this rich field of research.

2 Forces in the Actin Cytoskeleton

As it is the key player in cell motility and integrity, the actin cytoskeleton has been intensively studied on levels ranging from a single filament to groups of filaments (e.g. bundles, networks and gels) to the entire cytoskeleton (the whole cell). The first part of this chapter focuses on measurements of the actin-based force generation driving cell motility and a biomimetic model of the actin cortex, a quasi-two-dimensional network beneath the plasma membrane of eukaryotic cells.

Actin exists both in monomeric and polymerized forms. Actin filaments are 7-9 nm thick and are built up from the monomeric building block G-actin, a globular protein consisting of two domains. When G-actin concentrations are over 0.1 μM or the salt concentration is high, the G-actin starts to polymerize at the plus (aka barbed) end of the polar polymer, forming filamentous actin. This polymerization is not only responsible for the presence of filamentous actin in the cell, but is also the driving mechanism behind membrane protrusions (i.e. lamellipodia and filopodia) and bacterial locomotion. Unlike molecular motors, which consume chemically stored energy to generate forces, this so-called "brownian ratchet" or "polymerization motor" relies exclusively on Brownian motion (Peskin et al., 1993). Either the filament itself or the obstacle (e.g. the cell membrane) fluctuates according to its thermal motion, thereby generating a gap sufficiently large for another G-actin to be added to the growing filament in front of the obstacle (Figure 1). As the filament grows monomer by monomer, it exerts a force against the obstacle.

The forces generated by this mechanism have been studied both exper-

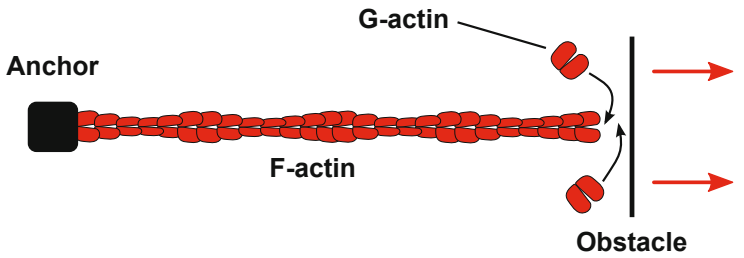

Figure 1. Schematic of the polymerization motor. The slow-growing (minus/pointed) end of the filament is anchored (black box), whereas at the fast growing (plus/barbed) end of the filament, addition of G-actin is still possible. An obstacle (black bar) limits the growth of the filament as soon as the gap between the growing filament and the obstacle becomes smaller than the size of a globular subunit. As the obstacle undergoes Brownian motion, the spacing becomes large enough for another subunit to be added. Therefore, the growing filament exerts a force (red arrows) along its axis pushing the obstacle.

imentally and theoretically. In addition to membrane protrusions in eukaryotic cells, pathogenic bacteria such as Listeria are believed to use the polymerization motor to move within a host cell. The pathogen presents ActA, a protein promoting actin polymerization, on its surface, inducing fast filament growth and movement. A minimal system of an ActA coated microsphere in an actin-rich cytoplasmic extract is sufficient to propel a 0.5 μm microsphere against the frictional force in medium with a speed of up to 0.2 μm/second (Cameron et al., 1999). A comet tail of several actin filaments behind the microspheres or bacteria is visible with both fluorescence imaging and electron micrographs (Brieher et al., 2004; Cameron et al., 1999). The question what force a single growing filament can contribute to this amazing propulsion can be calculated with

$$f = \frac{k_B T}{\delta} \ln\left(\frac{c}{c_c}\right) \tag{1}$$

where k_B is the Boltzmann factor, T the temperature, δ the gap size needed for an actin subunit to be added, c the concentration of G-actin and c_c the critical concentration (Peskin et al., 1993). It is also possible to measure the force of a single growing filament directly using optical tweezers (Footer et al., 2007). Optical tweezers are a versatile tool for force measurements in biology because they can sense forces from less than a piconewton

up to hundreds of piconewtons with high spatial resolution. In addition, they can be operated in biologically relevant medium to avoid damaging the specimen.

In one set of experiments, a bundle of actin filaments was attached to a microsphere trapped by optical tweezers and the force exerted by the polymerization motor against a rigid barrier was directly measured (Footer et al., 2007). The experimentally determined value of 0.76±0.22 pN corresponds very well with the calculated value of 0.8 pN for the maximum force (eq. 1).

It is also important that the growing semi-flexible filament can bear the force it exerts on the obstacle. In order to estimate the maximum force the filament can take before it buckles, one can use the Euler-Bernouille beam theory. The critical force at which a semi-flexible filament buckles is given by the critical Euler buckling force

$$f_{\text{crit}} = \frac{\pi^2 \cdot EI}{(KL)^2} = \frac{\pi^2 \cdot l_p k_B T}{(KL)^2} \tag{2}$$

where E is the elastic modulus, I the second moment of area, K a geometrical factor and L the length of the polymer. K depends on the condition of the ends of the polymer: In the case in Figure 1, one end is pinned to the anchor and the other is free to move laterally corresponding to $K = 2$. Replacing EI with the more common expression for semi-flexible polymers $l_p k_B T$, where l_p is the persistence length ($\approx 15\ \mu m$ for filamentous actin), gives a critical load of 0.15 pN for a 1 μm long actin filament. Therefore, it is clear that such a filament could not bear the load of 0.8 pN. However, the critical load of a bundle of filaments scales with N^α, where N is the number of filaments and α depends on the interconnection between the filaments. For weakly attached filaments, the force scales linearly with N ($\alpha = 1$), but for bundles bound by the actin binding protein (ABP) fascin, it scales quadratically ($\alpha = 2$, Mogilner and Rubinstein (2005)). This might be the reason for the fact that 10-30 parallel actin filaments bundled by fascin were found in filopodial protrusions (Figure 2) (Svitkina et al., 2003).

The next important issue to consider is how much force is needed to deform the cell membrane. Based on a Helfrich model, one can calculate the force of a cell membrane forming a cylindrical protrusion as

$$F = \frac{\kappa\pi}{R} + 2\pi R\sigma \tag{3}$$

where R is the radius of the protrusion, κ the membrane bending stiffness and σ the surface tension (Pronk et al., 2008; Nambiar et al., 2010). Using

$R = 200$ nm, $\kappa = 270$ pN nm and $\sigma = 0.003 \frac{\text{pN}}{\text{nm}}$, this equation gives a force of about 8 pN (Nambiar et al., 2010). This corresponds very well to the force of 10-30 filaments growing in a filopodium.

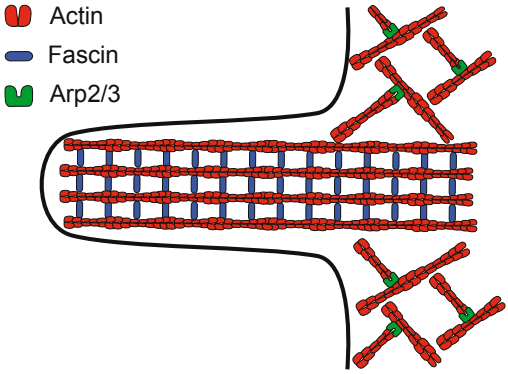

Figure 2. Schematic drawing of a filopodium. The cell membrane (black) is pushed by a growing bundle of several actin filaments (red). The filopodial actin filaments originate from a branched network of actin in the lamellipodium, which is organized by the Arp2/3 complex. Fascin (blue) bundles the filaments tightly, thereby greatly enhancing the mechanical stability of the bundle.

Another mechanism possibly driving membrane protrusions and bacterial locomotion has been proposed based on attractive interactions between two semi-flexible actin filaments in a splayed configuration and in contact with the obstacle being pushed (Figure 3) (Kühne et al., 2009; Streichfuss et al., 2011).

At the barrier the two filaments are splayed, whereas at the anchor they are bundled by an attractive interaction. This attractive interaction can be induced by counterion condensation along the negatively charged actin filament, ABPs, or the crowded cellular environment. In our group, we have used holographic optical tweezers (HOTs) to study the forces generated by the bundling of two individual actin filaments in such a geometry. Holographic optical tweezers use a diffractive optical element to alter the phase of the incoming laser beam in such a way that multiple traps are generated in the focal plane of the objective. These traps can be switched on and off, moved with high precision, tuned in intensity, and used as very sensitive force sensors. In combination with a microfluidic device, we can control the physical and chemical environment very precisely in order to study the influence of ionic strength on the force generation. The experiment started by

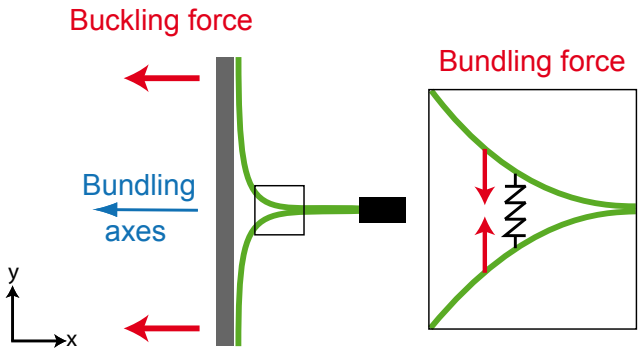

Figure 3. Schematic drawing of two actin filaments pushing an obstacle. Two actin filaments are anchored (black box) on one end. The opposite ends are splayed and in contact with the barrier to be pushed. The attractive interactions between the two filaments cause a force bundling them together (bundling force in the inset). Due to the semi-flexible nature of filamentous actin the bending is thereby increased and the buckled filaments exert a force along the bundling axes against the barrier (buckling force).

trapping three microspheres with HOTs, attaching two filaments to them in the configuration shown above, and then inducing the bundling with divalent ions (Figure 4). The forces driving bundle formation were measured by repeatedly changing the potential of the optical traps and recording the corresponding displacement of the microspheres (Figure 4B). After calibration of the optical traps, we could calculate the force exerted by the attractive interaction between the two filaments.

We also used a complementary approach to determine the forces during dynamic bundle formation. Having prepared the steady state condition described above, we switched off the optical traps for microspheres 1 and 2 (Figure 4A). Due to the attractive interaction, the filaments bundled and consequently pulled the microspheres against the viscous drag. Knowing the velocity of the dragged microsphere, we used the Stokes equation to calculate the generated force. These two complementary methods demonstrated independently that the forces generated depend on the concentration of divalent ions and can go up to 0.2 pN at 100 mM (Figure 5).

In addition to these fundamental measurements of the interactions between two filaments, we conducted experiments using multiple actin filaments on a scaffold of seven microspheres that resembles the actin cortex, a quasi two-dimensional network of actin beneath the plasma membrane

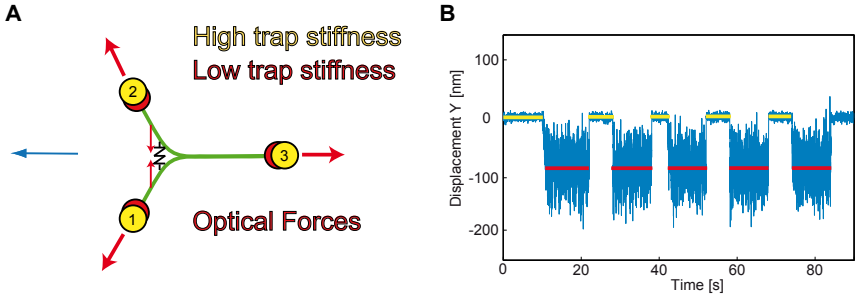

Figure 4. Schematic drawing of the experiment. First, we trap three microspheres with HOTs and attach two single actin filaments such that one is connected to microsphere 1 and 3, the other to microsphere 2 and 3. Subsequently, the bundling is induced by moving the filaments with the microspheres to a buffer with divalent ions, which results in bundling of the filaments along the bundling axes (blue) as far as the optical traps allow for. In this steady state, the optical forces (red) balance the attractive interaction. Next, the laser intensity and therefore the potential of the optical traps is alternately lowered and raised from ≈ 10 pN/μm (yellow) to ≈ 1 pN/μm (red), with simultaneous monitoring of the displacements of the microspheres. An example of the displacement of one microsphere is given in B.

(Uhrig et al., 2009). These seven microspheres were held by HOTs in a hexagonal array and subsequently filamentous actin was attached. Next, a buffer with 100 mM Mg^{2+} was introduced into an exchange chamber, allowing for the diffusion of the divalent ions into the experimental chamber. As soon as the ions reached the network, the filaments started to bundle and the networks contracted (Figure 6). Due to this contraction, the optically trapped microspheres were displaced, and the exerted force could be determined after trap calibration. These contractile forces increased as more and more ions diffused into the network, reaching up to 3 pN. This implies that more than 10 filaments were pulling on a microsphere, as previous experiments showed 0.2 pN per filament pair (Figure 6D). For the central microsphere the forces do not balance entirely as the filaments are not homogeneously distributed over the hexagon.

In summary, the measurements of force generation between two actin filaments during bundle formation revealed forces of up to 0.2 pN with 100 mM divalent ions, which is less than the force exerted by a single grow-

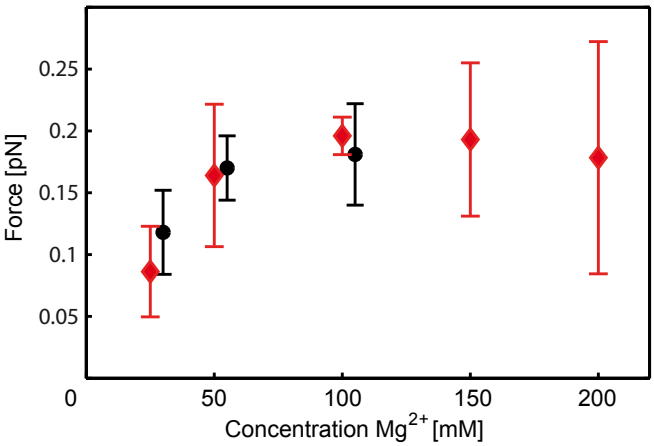

Figure 5. Forces generated by the bundling of two individual actin filaments, as measured by optical tweezers. The forces were measured in the steady state (red) and during dynamic bundle formation (black) using different concentrations of Mg^{2+} to induce counterion condensation along the negatively charged actin filaments. The forces are given by the mean ± standard deviation.

ing filament. However, while scaling of the buckling force with increasing number of filaments is expected and has been treated in theory, it has not yet been investigated experimentally (Kühne et al., 2009). A related experimental approach with 2D networks of actin filaments on a scaffold of 7 optically trapped particles in a hexagonal arrangement supports this idea, as the forces increased up to 3 pN for each of the trapped microspheres due to the large number of attached actin filaments (Uhrig et al., 2009).

3 Cell-Substrate Interactions

The actin network and the rest of the cytoskeleton are linked to the extracellular environment through large assemblies of proteins known as focal adhesions (Zamir and Geiger, 2001). Focal adhesions transmit information about the substrate to the actin network through transmembrane proteins called integrins. Integrins have both an extracellular component, which associates with proteins in the extracellular matrix surrounding the cell, and an intracellular component, which associates with the actin cytoskeleton

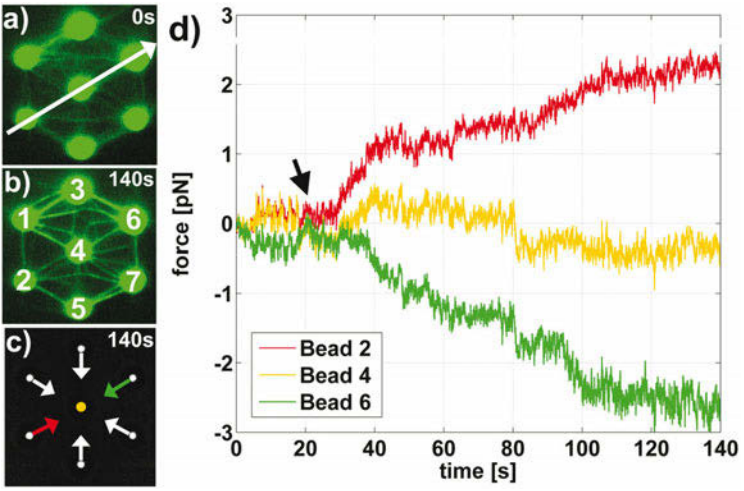

Figure 6. Experimental approach addressing the contractile forces in a quasi 2D actin network. A) Actin network with loosely hanging actin filaments on a hexagonal scaffold of microspheres optically trapped by HOTs. B) After diffusion of Mg^{2+} to the network the filaments start to bundle and contract the network. C) Schematic representation of the scaffold with the three microspheres colored red, yellow, and green, whose forces are shown in D. D) Forces exerted on microspheres 2, 4, and 6 by the contracting actin network during the bundling process induced by diffusion of Mg^{2+} ions to the network.

through focal adhesions. These linkages allow the cell to sense and respond to its mechanical environment (Giancotti and Ruoslahti, 1999). The information the cell receives about the substrate is transmitted throughout the cell via signaling pathways that can activate specific proteins or modify gene transcription. These signals (combined with others) influence whether the cell will grow, migrate, divide, differentiate, or even begin programmed cell death (Geiger et al., 2001).

The importance of this signaling is evident in the sensitivity of cells to the properties of the surface on which they are growing. Most cells from solid tissue must attach to a substrate before they are able to grow and divide. While there is a lot of variation between cell types, it can generally be said that cells attach more strongly to substrates with a similar stiffness to the tissue they came from (e.g. brain tissue 0.1-1 kPa and muscle 8-17 kPa) and in the presence of extracellular matrix proteins (Engler et al.,

2006; Ruoslahti and Pierschbacher, 1987). This has been nicely illustrated by plating cells on surfaces which have been micropatterned with specific shapes of adhesive molecules; the cells only adhered in the pre-coated regions and stress fibers (bundles of actin filaments) formed along the edges of the pattern (Théry et al., 2006).

However, many questions still remain about the precise nature of the cell-substrate interaction, particularly about the spatial arrangement of adhesion sites. It is difficult to perform studies on this topic because cells are constantly changing their environment by excreting extracellular matrix proteins and because many of the processes happen below the resolution limit of typical microscopy setups. In particular, researchers are interested in understanding better the role that integrin clustering plays in cell signaling. It has been shown that different signaling pathways are activated when only one integrin or a cluster of integrins is activated (Miyamoto et al., 1995), but the specifics of the receptor arrangement in these clusters is still not completely understood.

Towards this end, our group developed nanopatterned substrates that can present integrin-binding ligands with controlled densities and spacings (Girard et al., 2007; Cavalcanti-Adam et al., 2008). These surfaces are created through a technique known as block copolymer micelle lithography (BCML) (Lohmüller et al., 2011; Arnold et al., 2004). In the first step, gold salt-loaded micelles are created using block copolymers of polystyrene (PS) and poly-2-vinylpyridine (P2VP). Block copolymers are polymers with clearly defined segments comprising different monomer building blocks. In the block copolymers used here, the different components have dramatically different chemical properties: PS is nonpolar, while P2VP is polar. This heterogeneity within the copolymer leads to the formation of inverse micelles when the copolymer is dissolved in nonpolar toluene; the P2VP ends cluster together, creating a sphere with a polar core and a nonpolar shell. When a gold salt is added to this solution, the gold ions preferentially cluster in the polar cores. In the next step, a clean glass surface is dipped into the solution, generating a monolayer of micelles arranged in a hexagonal array as the glass slide is slowly removed from the micellar solution. It is important to precisely control the dipping speed in order to ensure well-ordered arrays.

This surface is then treated with an oxygen plasma, which reduces the gold salt to generate solid gold nanoparticles between 1 and 12 nm in diameter, depending on the amount of gold salt loaded. The plasma treatment also removes the excess solvent and the copolymer from both the gold nanoparticles and the glass substrate. This technique is capable of producing gold nanoparticle arrays with well-defined inter-particle distances and

a high degree of order, as shown in Figure 3. The inter-particle distance can be tuned between 30 and 250 nm by tuning the copolymer composition, concentrations, and the dipping speed (Spatz et al., 2000; Lohmüller et al., 2011).

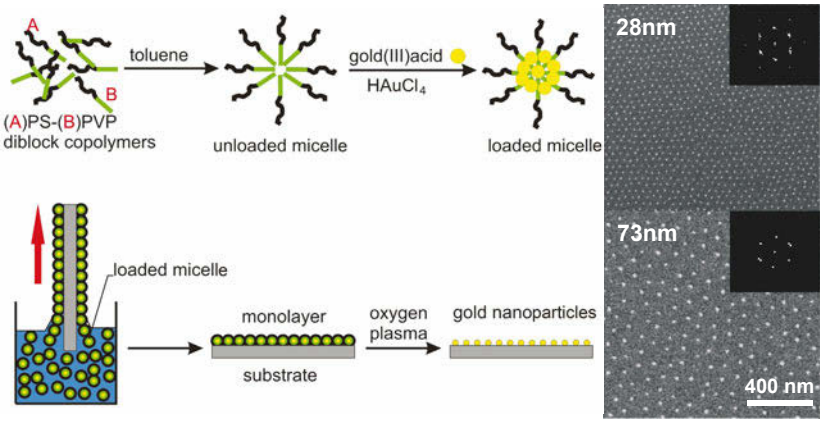

Figure 7. Block copolymer micelle lithography. Clean surfaces are coated with a monolayer of gold ion-loaded micelles by dipping the substrate under precisely controlled conditions. After treatment with an oxygen plasma, the surfaces are patterned with a precise array of gold nanoparticles.

We chose to create the nanoparticle arrays with gold due to the high biocompatibility and well-known surface chemistry of this metal. Thiol group-containing compounds (R-SH) bind readily to gold and have been used to attach a wide variety of biologically active components to gold surfaces and nanoparticles. For integrin-related experiments, we conjugate the nanoparticles with a cyclic-RGD peptide containing a thiol group at the end of a short alkane spacer. The RGD amino acid sequence (Arginine-Glycine-Aspartic acid) is commonly found in extracellular matrix proteins and is known to bind to integrin receptors (Ruoslahti and Pierschbacher, 1987). Cells typically adhere readily on surfaces displaying these amino acid sequences. By placing these peptides only on the surface of the nanoparticles, we can study how the spacing of RGD ligands affects the cell's response. As the cross-section of an integrin is 10-12 nm, when small gold nanoparticles are used (e.g. 5-8 nm), it can be assumed that only one integrin can bind to each nanoparticle (Figure 8A) (Arnold et al., 2004). Therefore, the spacing of the gold nanoparticles on the surface controls the closest distance two

integrins can obtain, consequently controlling their clustering density. In order to ensure that the ECM proteins secreted by the cell do not adsorb onto the glass between the nanoparticles and lead to non-specific interactions, these regions are passivated with covalently-bound poly(ethylene glycol) (PEG), which repels proteins and provides a neutral background (Bluemmel et al., 2007). With this setup, the cells can only interact with the surface through the nanopatterned RGD peptides. The specific interaction between the cell and the RGD peptides on the gold nanoparticles was observed in SEM images of cells fixed after they had adhered to nanopatterned surfaces (Figure 8B). Protrusions extend from the edge of the cell to the nanoparticles (visible due to dehydration during the fixing process), but not to the surface in between.

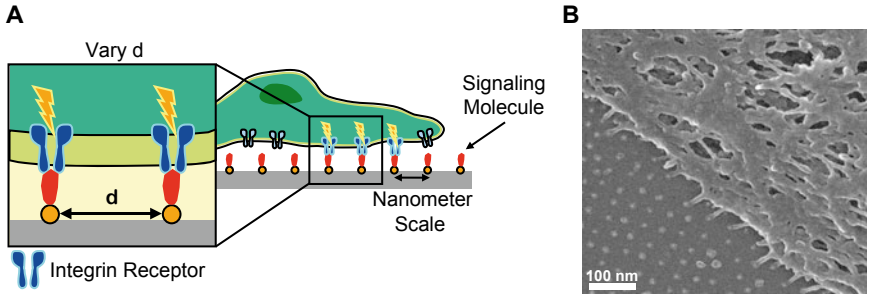

Figure 8. A) Integrins are 10-12 nm in size and therefore only one integrin can bind to one gold nanoparticle, which has a size of 5-8 nm. The interparticle distance on the surface also controls the closest spacing two integrins can have when cells adhere. B) The interaction of the cell with the gold nanoparticles and not the PEG-passivated background can be seen under the SEM.

The importance of integrin clustering for cell adhesion was studied by plating rat embryonic fibroblast (REF) cells on RGD-functionalized nanopatterned surfaces with different gold nanoparticle spacings. When the distance between the gold nanoparticles was less than 60 nm, a large number of cells could adhere to the surface. However, when the spacing was larger than 70 nm, the number of cells that could adhere was greatly reduced (Figure 9A). Differences could also be seen on the single cell level; cells on surfaces with gold nanoparticle spacings under 60 nm had a larger spreading area and were more circular in shape. Furthermore, when the cells were stained for the integrin β_3 (blue), the focal adhesion protein vinculin (red) and the actin

cytoskeleton (green), cells on surfaces with spacings under 60 nm showed colocalization of vinculin and integrin β_3, indicating the formation of mature focal adhesions. The formation of the focal adhesions resulted in the establishment of distinct stress fibers in the actin cytoskeleton, which were also only observed on the surfaces with particle spacings below 60 nm (Figure 9C-D) (Cavalcanti-Adam et al., 2006). The cells on the surfaces with a larger spacing had contact with only a few spots on the surface, were more triangular in shape, had a smaller spreading area and didn't form mature focal adhesions (i.e. vinculin and integrin β_3 stains were diffuse and did not colocalize) (Figure 9C-D). From this data we concluded that integrins need to cluster closer together than 60 nm for mature focal adhesions to form (Figure 9B) (Arnold et al., 2004).

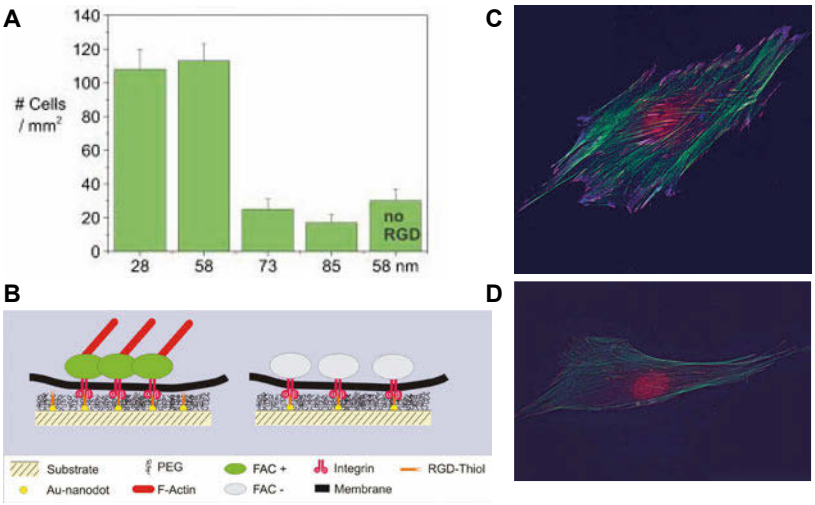

Figure 9. Adhesion of cells on gold nanopatterns with different particle spacings. A) Cells adhere well on surfaces with inter-particle distances lower than 60 nm but not on surfaces with larger particle spacings. B) Mature focal adhesions can form and connect to the actin skeleton on surfaces where the integrins can cluster closer than 58 nm. Focal adhesions cannot form when the spacing of integrins is larger than 73 nm. Overlayed images of cells on surfaces with 58 nm (B) and 109 nm (C) inter-particle spacing stained for integrin β_3 (blue), vinculin (red), actin (green).

Cells can sense not only the overall spacing but also gradients of the adhesion ligand RGD (Hirschfeld-Warneken et al., 2008). The spacing of

gold nanoparticles can be varied on a glass surface by changing the speed the glass is removed from the gold micellar solution. By pulling with a constant acceleration, gradients of gold nanoparticles with a controlled steepness can be formed. Cells were plated on such surfaces with 15 nm/mm gradients (i.e. the inter-particle distance changes 15 nm per mm on the slide), resulting in a spacing that increased from 60 nm up to 100 nm. On these surfaces, cells were able to sense the gradient and moved towards the closer-spaced part of the surface, thereby adopting a polarized shape. Based on the size of a cell and the steepness of the gradient, this means that the cell can sense a difference of less than 1 nm in the ligand spacing between the opposing ends of the cell. Interestingly, the cell adhesion behavior on ordered vs. randomly patterned gold nanoparticle surfaces was strikingly different (Huang et al., 2009). To study this phenomenon in detail, four surfaces were prepared with gold nanoparticles with high density ordered, high density random, low density ordered and low density random patterns (Figure 10A). Cells showed similar adhesion to surfaces with a high ligand density whether the particles were ordered or random. However, at low particle densities, cells couldn't adhere to the ordered substrates, while the cells were able to adhere if the nanoparticle arrangement was random (Figure 10B). Thus, even if gold nanoparticle, and therefore adhesion molecule densities, are low on a global level, the cell can adhere if localized clusters can be formed.

As becomes clear from the comparison between ordered and random patterned surfaces, not the global but the local clustering of integrins is critical for the formation of an adhesion cluster. Therefore, the question becomes how many integrins are required in a cluster for one stable focal adhesion to form (Arnold et al., 2009). To answer this question, we have to control the spacing of the gold nanoparticles not only on the nanometer length scale but also on the micrometer length scale. To produce such surfaces, a combination of the above described BCML technique and photo/e-beam lithography was used (Figure 11A). In short, the gold nanostructured glass surfaces prepared by BCML were coated with a photo-sensitive resist which can be etched away by a light/e-beam into μm-sized patterns. Nanoparticles that are no longer protected by the resist can selectively be removed. Finally, the rest of the resist is also removed, yielding nanopatterned microstructures on glass.

Nanopatterns with 58 nm gold nanoparticle spacings were divided into 150 x 150 μm patches with square micropatterns (3000 nm, 1000 nm, 500 nm, 250 nm and 100 nm in side length) that were separated by their respective side length (Figure 11B). Therefore, the number of gold nanoparticles in each square was controlled by the size of the square micropattern, and the number of gold particles per square was 3000, 300, 80, 30 or 6.

A

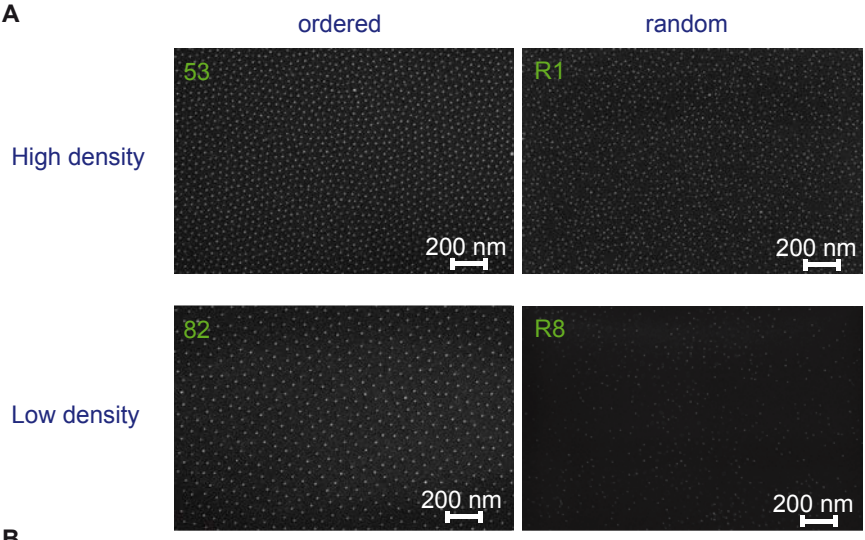

B

Pattern	Au nanoparticle density (μm^{-2})	Average Interdot Spacing±Standard Deviation (nm)	**Cell Adhesion**
R1: Random High density (1)	408 ± 32	55 ± 14	**YES**
R8: Random Low density (2)	151 ± 39	83 ± 33	**YES**
53: Ordered High density (3)	416 ± 20	53 ± 8	**YES**
82: Ordered Low density (4)	171 ± 16	82 ± 12	**NO**

Figure 10. Cell adhesion on ordered vs. random gold nanoparticle patterns. A) SEM images of the prepared surfaces. B) Characterization of the ordered and randomly patterned surfaces.

Despite the dramatically reduced global nanoparticle density, the cells were able to adhere to these micro-nanopatterns. However, differences were observed. In the case of the larger patches with 3000 and 300 gold nanoparticles per patch, formation of classical focal adhesions on the patches was observed. (Figure 11C) On the other hand, while the cells were still able to adhere to the smaller patches, with 80, 30 or 6 nanoparticles per patch, elongated adhesions bridging several patches were observed (Figure 11D). When the number of gold nanoparticles in a square was lower than 6 per

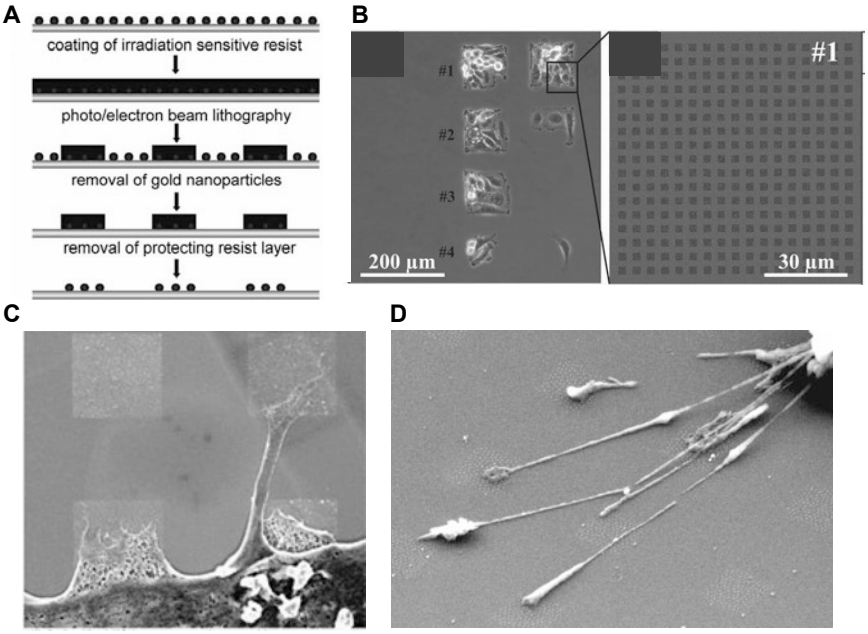

Figure 11. Cell adhesion on micro-nanopatterned gold nanoparticle surfaces. A) Preparation of micropatterns. B) Micropattern on the surfaces. C) Cells on nanostructured 3000 x 3000 nm micropatterns. D) Cells on nanostructured 250 x 250 nm micropatterns.

patch, the cells could not form stable focal adhesions, which shows that 6 is the minimum number of integrins that have to cluster in order to form a stable focal adhesion. Together these experiments help shed a light on the complex interactions between cells and their substrates. Through the use of carefully designed nano- and micro-structured materials, we were able to show that two integrins have to be closer than 60 nm for the cell to adhere to the substrate, that cells are able to sense small differences in ligand concentration and move toward greater ligand densities, and that at least 6 integrins must cluster together to form a stable focal adhesion.

4 Conclusion

Experiments such as those presented here have given biologists a clearer picture of the forces found in native biological systems and given them more

powerful tools to influence cell behavior. This type of knowledge could be helpful in designing better materials for a variety of biomedical applications and could make it possible to encode signals into surfaces in order to direct cell behavior.

Bibliography

Bruce Alberts, Alexander Johnson, Julian Lewis, Martin Raff, Keith Roberts, and Peter Walter. *Molecular Biology of the Cell*. Garland Science, New York, 5 edition, July 2008.

Marco Arnold, E Ada Cavalcanti-Adam, Roman Glass, Jacques Blümmel, Wolfgang Eck, Martin Kantlehner, Horst Kessler, and Joachim P Spatz. Activation of Integrin Function by Nanopatterned Adhesive Interfaces. *ChemPhysChem*, 5(3):383–388, January 2004.

Marco Arnold, Marco Schwieder, Jacques Bluemmel, E Ada Cavalcanti-Adam, Monica Lopez-Garcia, Horst Kessler, Benjamin Geiger, and Joachim P Spatz. Cell interactions with hierarchically structured nanopatterned adhesive surfaces. *Soft Matter*, 5(1):72–77, January 2009.

Jacques Bluemmel, Nadine Perschmann, Daniel Aydin, Jovana Drinjakovic, Thomas Surrey, Monica Lopez-Garcia, Horst Kessler, and Joachim P Spatz. Protein repellent properties of covalently attached PEG coatings on nanostructured SiO(2)-based interfaces. *Biomaterials*, 28(32):4739–4747, November 2007.

William Brieher, Margaret Coughlin, and Timothy Mitchison. Fascin-mediated propulsion of Listeria monocytogenes independent of frequent nucleation by the Arp2/3 complex. *The Journal of Cell Biology*, 165(2): 233–42, 2004.

Lisa Cameron, Matthew Footer, Alexander van Oudenaarden, and Julie Theriot. Motility of ActA protein-coated microspheres driven by actin polymerization. *Proceedings of the National Academy of Sciences of the United States of America*, 96(9):4908–13, April 1999.

E Ada Cavalcanti-Adam, Alexandre Micoulet, Jacques Bluemmel, Jörg Auernheimer, Horst Kessler, and Joachim P Spatz. Lateral spacing of integrin ligands influences cell spreading and focal adhesion assembly. *European Journal of Cell Biology*, 85(3-4):219–224, January 2006.

E Ada Cavalcanti-Adam, Daniel Aydin, Vera Catherine Hirschfeld-Warneken, and Joachim P Spatz. Cell adhesion and response to synthetic nanopatterned environments by steering receptor clustering and spatial location. *HFSP Journal*, 2(5):276–285, October 2008.

Adam J Engler, Shamik Sen, H Lee Sweeney, and Dennis E Discher. Matrix Elasticity Directs Stem Cell Lineage Specification. *Cell*, 126(4):677–689, August 2006.

Matthew Footer, Jacob Kerssemakers, Julie Theriot, and Marileen Dogterom. Direct measurement of force generation by actin filament polymerization using an optical trap. *Proceedings of the National Academy of Sciences of the United States of America*, 104(7):2181–6, February 2007.

Benjamin Geiger, Alexander Bershadsky, Roumen Pankov, and Kenneth M Yamada. Transmembrane crosstalk between the extracellular matrix-cytoskeleton crosstalk. *Nature Reviews Molecular Cell Biology*, 2(11): 793–805, November 2001.

Filippo G Giancotti and Erkki Ruoslahti. Integrin Signaling. *Science*, 285 (5430):1028–1033, August 1999.

Philippe P Girard, E Ada Cavalcanti-Adam, Ralf Kemkemer, and Joachim P Spatz. Cellular chemomechanics at interfaces: sensing, integration and response. *Soft Matter*, 3:307–326, January 2007.

Vera Hirschfeld-Warneken, Marco Arnold, E Ada Cavalcanti-Adam, M Lopez-Garcia, Horst Kessler, and Joachim P Spatz. Cell adhesion and polarisation on molecularly defined spacing gradient surfaces of cyclic RGDfK peptide patches. *European Journal of Cell Biology*, 87(8-9):743–750, June 2008.

Hayden Huang, Roger D Kamm, and Richart T Lee. Cell mechanics and mechanotransduction: pathways, probes, and physiology. *AJP: Cell Physiology*, 287(1):C1–C11, February 2004.

Jinghuan Huang, Stefan V Grater, Francesca Corbellinl, Sabine Rinck, Eva Bock, Ralf Kemkemer, Horst Kessler, Jiandong Ding, and Joachim P Spatz. Impact of Order and Disorder in RGD Nanopatterns on Cell Adhesion. *Nano Letters*, 9(3):1111–1116, January 2009.

Paul A Janmey. The cytoskeleton and cell signaling: component localization and mechanical coupling. *Physiological Reviews*, 78(3):763–781, July 1998.

Simon Jungbauer, Huajian Gao, Joachim P Spatz, and Ralf Kemkemer. Two Characteristic Regimes in Frequency-Dependent Dynamic Reorientation of Fibroblasts on Cyclically Stretched Substrates. *Biophysical Journal*, 95(7):3470–3478, October 2008.

Torsten Kühne, Reinhard Lipowsky, and Jan Kierfeld. Zipping mechanism for force generation by growing filament bundles. *Europhysics Letters*, 86(6):68002, 2009.

Theobald Lohmüller, Daniel Aydin, Marco Schwieder, Christoph Morhard, Ilia Louban, Claudia Pacholski, and Joachim P Spatz. Nanopatterning by block copolymer micelle nanolithography and bioinspired applications. *Biointerphases*, 6(1):MR1, 2011.

Shingo Miyamoto, Steven K Akiyama, and Kenneth M Yamada. Synergistic roles for receptor occupancy and aggregation in integrin transmembrane function. *Science*, 267(5199):883–885, February 1995.

Alexander Mogilner and Boris Rubinstein. The physics of filopodial protrusion. *Biophysical Journal*, 89(2):782–95, 2005.

Rajalakshmi Nambiar, Russell McConnell, and Matthew Tyska. Myosin motor function: the ins and outs of actin-based membrane protrusions. *Cellular and Molecular Life Sciences*, 67(8):1239–54, 2010.

Charles Peskin, Garret Odell, and George Oster. Cellular motions and thermal fluctuations: the Brownian ratchet. *Biophysical Journal*, 65(1): 316–324, 1993.

Sander Pronk, Phillip Geissler, and Daniel Fletcher. Limits of Filopodium Stability. *Physical Review Letters*, 100(25):4–7, 2008.

Erkki Ruoslahti and Michael D Pierschbacher. New Perspectives in Cell-Adhesion - RGD and Integrins. *Science*, 238(4826):491–497, 1987.

Joachim P Spatz, Stefan Mössmer, Christoph Hartmann, Martin Möller, Thomas Herzog, Michael Krieger, Hans-Gerd Boyen, Paul Ziemann, and Bernd Kabius. Ordered Deposition of Inorganic Clusters from Micellar Block Copolymer Films. *Langmuir*, 16(2):407–415, January 2000.

Martin Streichfuss, Friedrich Erbs, Kai Uhrig, and Rainer Kurre. Measuring Forces between Two Single Actin Filaments during Bundle Formation. *Nano Letters*, 11(9):3676–80, September 2011.

Tatyana Svitkina, Elena Bulanova, and Oleg Chaga. Mechanism of filopodia initiation by reorganization of a dendritic network. *The Journal of Cell Biology*, 160:409–421, 2003.

Manuel Théry, Anne Pépin, Emilie Dressaire, Yong Chen, and Michel Bornens. Cell distribution of stress fibres in response to the geometry of the adhesive environment. *Cell Motility and the Cytoskeleton*, 63(6): 341–355, June 2006.

Kai Uhrig, Rainer Kurre, Christian Schmitz, Jennifer E Curtis, Tamás Haraszti, Anabel E-M Clemen, and Joachim P Spatz. Optical force sensor array in a microfluidic device based on holographic optical tweezers. *Lab on a chip*, 9(5):661–8, March 2009.

Eli Zamir and Benjamin Geiger. Molecular complexity and dynamics of cell-matrix adhesions. *Journal of Cell Science*, 114(20):3583–3590, 2001.